Heliyon 10 (2024) e33743

Contents lists available at ScienceDirect

Heliyon

journal homepage: www.cell.com/heliyon

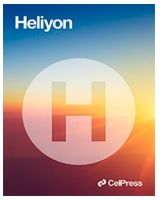

Research article

New approach for processing chitosan as low cost protective hybrid coating for C-steel in acid media

Salam N.Hattawi [a], Ahmed G. Ahmed [b], Firas M. Fadhil [b], Stephen R. Kuot [c], Mai S Alsubaie [c], Mohammed L.Alazmi [c], H.A. Fetouh [c,*]

[a] Northern Technical University, College of Health and Medical Techniques, Department of Renal Diaylsis Techniques, Kirkuk, Iraq
[b] University of Kirkuk, College of Education for Pure Science-chemistry Department, Kirkuk, Iraq
[c] Chemistry Department, Faculty of Science, Alexandria University, Egypt

ARTICLE INFO

Keywords:
Hybrid coating
Chitosan
Coated silica
Protective
Carbon steel

ABSTRACT

The novelty of this study is that it the first time blending and formulation of chitosan as a new hybrid (organometallic) protective coatings for achieving synergistic protection for carbon steel alloy during acid pickling. The role of coated silica (by 0.1 wt % stearic acid lubricant) in the improvement of coating performance was highlighted. Variable weight percentage of chitosan and silica in addition to a fixed weight percentage (35 %) of guar gum natural plant resin, 5×10^{-6} mmol (2-Hydrazinyl-6-methyl (or phenyl) −4, 5-di-H pyrimidinone) as organic corrosion inhibitors were compounding as hot melt in the presence of a low cost surfactant as an emulsifying agent improved compatibility between coating constituents. Guar gum increased coating flow during application and grafted chitosan into high molecular copolymer resin insoluble in acid media. Phosphorous acid improved coating flexibility during application by hot dipping. Hybrid coating decreased corrosion potential of carbon steel and retarded both redox reactions of corrosion acting as adsorbed mixed-type inhibitor. Percentages protection (%P) approached hundred percentage as confirmed from the agreement between impedance and polarization parameters. Guar gum plant resin and slice powder increased gloss of coating. The coated silica filled the pores and increased stiffness of coating. Super hydrophobicity of coating was confirmed by the measured contact angle above 150°C indicating good spreading of coating sample as insulating adherent surface film.

1. Introduction

Corrosion control by cathodic, anodic protection required coating metal (M) surface by anticorrosive protective coating [1]. Hybrid coatings forms barrier protective non-porous adherent surface film resist moisture) [2], isolate M surface from corrosive environment. Intrinsic strength improved durability. Film thickness and content affect protection lifespan. Resist impact and cracking, maintain appearance when exposed to mechanical stress (expansion, or weathering). Performance, durability depend on composition (binders, pigments, solvents, extenders, type& pretreatment M surface, curing conditions (heating, chemical reactions, radiation, etc.), film thickness, adhesion, corrosive environment [3].

Challenges in organic coating are [4–6]: photo-degradation, require oxygen for curing, ester primers binder experience (gelling on

* Corresponding author.
E-mail address: howida_fetouh@alexu.edu.eg (H.A. Fetouh).

https://doi.org/10.1016/j.heliyon.2024.e33743
Received 23 February 2024; Received in revised form 25 June 2024; Accepted 26 June 2024
Available online 27 June 2024

aging, alkaline hydrolysis under no precautions). Less protective single layer: weak mechanical strength, thermally degradation above 150 °C. Polymer thermosetting resin (reservoir (vehicle) hold corrosion inhibitors) anti-corrosive coating →good barrier properties, properties easily modified, formulated. Limitations: poor resistance to (crack initiation, propagation, abrasion, wear. Cracks allow penetration of water, oxygen and ions to M surface causing corrosion [7,8]. Inorganic coating: porous, have residual stress (stress-induced cracks allow diffusion of corrosive species to M surface). Metallic coatings of Cr; Zn; Ni; Al, and Cu involved toxic pollutants [9].

Hybrid organic inorganic coating is protective for metals and alloys in many aggressive environment. It is formulated as: Binder (polymer resins such as epoxy, polyester, acrylic), Nano filler and additives. Nano-fillers (CNT TiO_2, NPs (ZnO (improved corrosion resistance), toughness (inhibited fracture), Al_2O_3 (improved corrosion resistance, adhesion). Silica improved wear resistance and adhesion [10,11]. Silica coated by stearic acid lubricant increased hydrophobicity coating by inducing surface roughness. Hydrophobicity increases with reducing surface free energy of metal//air interface (γSV). Surface roughness decrease wetting of coated metal surface by aqueous media. The apparent contact angle on rough surface calculated by equation [12]:

$$\text{Cos}\,\theta w = r\cos\theta \tag{1}$$

The *angle* θw can be observed by the naked eye or by using an optical microscope; and *r* is the ratio between the actual surface area to the apparent selected area (roughness factor(r) is more than one for a rough solid surface; θ is the CA of the corresponding smooth surface. On hydrophobic coating, water droplet has a larger CA on a rough surface compared to the corresponding smooth one ($\theta w > \theta > 90^{\circ}$). Rough traps air gases in the grooves present between the cauliflower clusters. Air enhanced water repellency and elevates water contact angle [13].

Polymer resin require additives with definite physicochemical properties to improve physicochemical (control specific applications) [14–16]: Enhanced (abrasion resistance, adhesion, and wetting), fill pores (decreased water penetration& ester hydrolysis, biodegradation and affected hot melt polymers flow by improving rheology). Additives improved aesthetics, wear resistance, application, thermal stability, impact resistance, flame retardation, decrease photo degradation. Reinforcing fibers (substance of high strength, inert as C, glass fibers) decreasing thermal expansion, enhancing mechanical strength, may increasing density, decreasing impact and costs, increase stiffness. Blended with binder during compounding without changing molecular structure, formulation design according to property require enhancement. Inorganic or organic, natural or synthetic substance enhance mechanical strength, rheology, structure; effectiveness depends on chemical structure molecular weight and melting point [17]. Formulation of hybrid coating is a new state of art need scaling up to conserve and protect resources of metals against corrosion.

Chitosan is a nature available polymer required grafting and several additive before commercialization as protective hybrid coating. *Chitosan* grafted by Refs. [18,19]: acrylic acid-, 2-acrylamido-2-CH_3-propane-H_2SO_3); 4, 4′-oxy-dianiline-formaldehyde-carbohydrazide); di-isopropyl fumarate; vinyl benzoate; 2-OH-ethyl methacrylate; 5-benzyloxy-4-oxo-4H-pyran-2-yl-CH_3 acrylate-acrylic acid; kojic acid/acrylic acid; acyl, OH/COOH)-alkyl, glycerol PO_4, acrylamide groups, thiol (SH) and sulphure (S) compounds, copolymerization, crosslinking; oleic acid lubricant and graphene oxide filler [14]; hydrophobic coating stearic acid coated silica (photo thermal stability); silica-PO_4; poly di-CH_3 siloxane (protected steel in NaCl [16]; hydrophobic durable coating Al-PO_4 adhesive@polydi-CH_3-siloxane modified by per-F-decyl-tri-ethoxysilane; epoxy resin di-glycidyl ether bisphenol-silica [18] and glycydoxy-tri-methoxy/ethoxy silane [19–23].

The hybrid coating of chitosan silica showed many issues in adherence, durability, porosity and inadequate studies [24] for C-steel. All investigation were restricted to flammability retardation by phosphide –nitrogen double bond and photo degradation. Hence this current study aims blending (chitosan as insoluble binder), application and characterization of new CT into protective hybrid coating from chitosan coated silica (1.5 mμ) for C-steel during acid pickling.

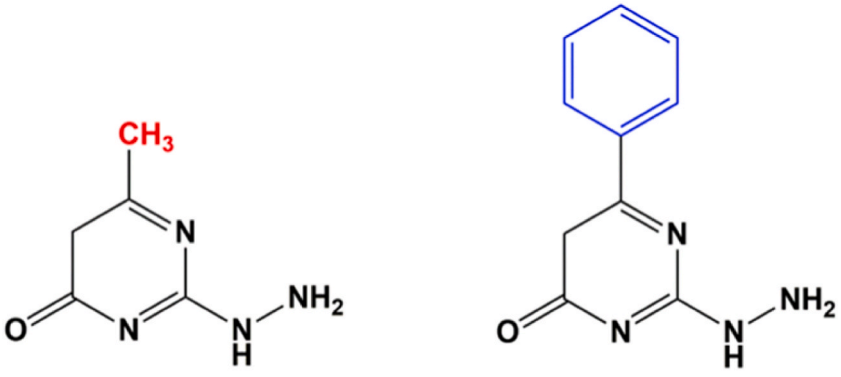

Fig. 1. Chemical structure:2-Hydrazinyl-6-CH3/Ph-4,5-di-H-pyrimidinon.

2. Experimental

2.1. Material and methods

All chemicals were pure and purchased from Sigma Aldrich Co. Hydrochloric acid, HCl (36 % wt.). Chitosan (weight molecular weight, Mw. 300 k Da, 85 % deacetylation degree, guar gum (for improving rheology and corrosion resistance). Traces aiding additives are anionic surfactant Na dodecyl sulphate as wetting and dispersion agent, alkali soda improved CT film. Phosphorous acid stabilizer and plasticizer, tri phenyl phosphonium chloride (TPPC), Methyl or phenyl pyrimidinon (corrosion inhibitors have similar chemical structure and abbreviated as MePyr, PhPyr, Fig. 1 for chemical grafting of chitosan

Coated silica (particle size 1.5 mμ) contains many oxides: 24.0 % Na, 25 % Ca, 5 % P and the remainder SiO_2 coated by 1.0 wt % stearic acid. Fig. 2 represented coating constituents.

2.2. Formulation of the hydrophobic coating (hybrid coat formulation)

The main coating constituents was collected in Table 1.

The Wt. % of guar gum was fixed at 35 % (Above and below this wt.35 %, coating formed semisolid and solid gel made grafted chitosan became unsuitable binder resin. Constant wt. % of coating aids are: TPPC provided soft Lewis base P atom, ph groups extending electron delocalization; H_3PO_3 (3 mL) for adherent primer phosphating and film elasticity. pH adjusted alkaline by using 20 mL 0.5 M NaOH to attain CT film, 10 mL CH_3 or Ph pyrimidinon and 10 mL 0.5 M SDS emulsifying agent in 50 mL water. Coatings were prepared as hot melt *via* agitation at 100 rpm, 110°C for one-half hour till homogenous flow obtained.

Working electrode (WE) is steel with element analysis (wt.%): 1.18%C, 84%Mn, 0.01%P, 0.005 %S, 0.02%Cu, 0.02%Cr and 97.93 iron, surface area 1.89 cm^2 [24]. Metal surface was mechanically polished using different grades emery papers starting by coarse grade (320) and proceeding to the finest grade (1000) till achieving metallic luster; rinsed thoroughly with double-distilled water, ethanol and dried before coating application by hot dipping and heat cured at 80°C in electric oven for 4.0 h through simple chemical reaction and crosslinking [25].

Coating samples were characterized. FTIR spectra (KBr pellets) using calibrated Bruker TENSOR 37 spectrophotometer 1430 at frequency range 4000-450 cm^{-1}; surface morphology using sanning electron microscope JSM-IT200 SEM [22]. Thermogravimetric (TGA),- and differential thermal (DSC) analysis at heating rate 10 °C.min^{-1} under inert nitrogen using Shimadzu DTA/TGA-50. The average particle size distributions of some diluted suspended coating samples in double distilled water samples are determined using photon spectroscopy dynamic light backscattering: angle 173° at 25.0 ± 0.1 °C [26].

In evaluation of biocide activity, a volume 30 mL 100 ppm 10%CT is chemically grafted at primary OH, NH_2 by 10 mL, 10^{-4} M CH_3/Ph pyrimidinone using sonochemical method at 20 kHz for an hour till complete homogeneity. The overheating and high pressure in liquid bubbles enhanced grafting reaction. The native and grafted CT were evaluated as biocides against different biofilms *via* determination the minimum inhibitory concentration (MIC: the lowest concentration stop growth) by twofolds serial dilution (62.5, 125, 250, 500 from 1000 μg/mL sample dissolved in 10 mL double distilled water following Clinical and Lab. Standards Institute guidelines (2018). Biofilm cultured (100 μL Muller-Hinton broth (MHB) (Oxoid® Limited, Basingstoke, UK) in agar plates. A volume 100 μL test sample added (5, 25, 50 and 100 ppm to culture mixtures, incubation at 37°C for a day with amoxicillin 1000 μgmL^{-1} reference standard antibiotic. Microorganism culture is diluted ten time by demineralized water to get 1×10^6 colony forming unit mL^{-1}. Two concentrations "1", "2" ; 250 μL each sample is placed on agar plates using glass beads. For each biofilm, positive and negative controls were applied [27].

The bare and coated samples were evaluated during acid pickling by electrochemical measurement carried out in three electrodes 50 mL glass cell. The WE was either bare or coated metal surface. Counter (CE) was Pt allow current flow. Reference electrode (RE) saturated calomel SCE was placed into Luggin capillary at 3 mm distance to WE to eliminate Ohmic overpotential. Cell and its

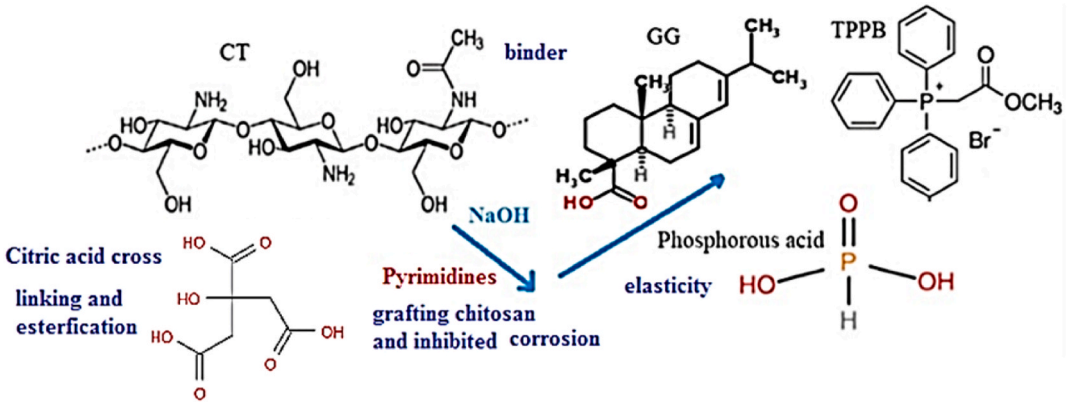

Fig. 2. The main chemical constituents of chitosan hybrid coating.

Table 1
Chemical constituents of coating samples.

CT	65	64	63	62	61	Sample 5+MePyr	Sample 5+PhPyr
Coated silica	–	1	2	3	4	5×10^{-6} mmol	
Sample No.	1	2	3	4	5	6	7

components were carefully cleaned after each run, washed with tap-, double-distilled water and a portion test solution [2]. 1.0 M HCl test solutions were diluted from 4.0 M HCl solution (6.25 mL 4.0 M HCl completed to 25 mL double distilled water. The cell was connected to Gamry potentiostat reference 600 sequencer and thermostated at 60°C, Fig. 3 [28].

Reversible rest potential (E_{rev}) of WE was established for reliable electrochemical measurements. AC polarization 10 mV amplitude signal from 1 Hz 100 kHz at E_{rev}. Echem analyt V6.20 was used for data analysis. DC polarization voltage was ±250 mV around E_{rev}, sweep rate 1 mVs^{-1}. Corrosion rate (C.R) equals corrosion current density (i) and (1/Rct) obtained from DC and AC polarization. Protectage protection (%P) was calculated by using equation (1) [28].

$$\text{Percentage protection, } \%P = \frac{Rct - Rcto}{Rct} \times 100 = \frac{i_o - i}{i} \times 100 \quad (2)$$

Where i_o, R_{cto} and i, Rct are corrosion current density and charge transfer resistance of bare and coated sample respectively.

Contact angle was measured using static method and direct measurement of the tangent angle at the three-phase contact point on a sessile 5.0 μL water droplet [10]. Wetting coated metal by water was identified by depositing water droplet on metal surface and measuring the wetting contact angle (WCA) using static method and direct measurement of the tangent angle at the three-phase contact point on a sessile small-volume water drops 5.0 μL profile optical tensiometers (goniometers), Apex instrument [29], Fig. 4.

Coating porosity measured as: coated metal sample was air emptied using BELPREP- vacuum II, BEL Japan, Inc. at 300°C for 3h, placed in a porosity analyzer (BELPREP-mini 2, BEL japan, Inc. with 99.99 % pure adsorbed nitrogen at 77 K. Internal surface area, S_{BET}, total pore volume mean diameter were calculated using Brunauer-Emmett-Teller (BET) linear plots [30].

3. Results and discussion

FTIR spectra, representative in Fig.SI1 confirmed successful bonding intercalation among coating constituents. Characteristic vibrational absorption bands of functional groups were assigned as: 3440.64–3111 (NH, OH symmetric stretching,NH_2, 3111.94, 2956.99 (asymmetric stretch CH_2, 1645.25 (carbonyl), C═O, NH_2 asymmetric stretching. 2888.67 (NH asymmetric stretching), 2131.92 (CH), 750-679 (bending, wagging carbonyl bond of carboxylic group, (2986 cm^{-1}C–H), 1424 cm^{-1}, rocking 1078.52 O–H of chitosan, 466 cm^{-1}-588 cm^{-1} O–Si–O bending; Si–O–Si 1033 cm^{-1}stretch; 925 cm^{-1}-948 cm^{-1}Si–O_2 nonbonding orbitals, 478 cm^{-1}-486 cm^{-1}Si–O–Si rocking; 771 cm^{-1}-779 cm^{-1}Si–O–Si bending, 2329.39Asym. NH_3^+, 1762 cm^{-1}ester, 1787.90 (ester), hydrogen bonds (1073- 897), 470.19 cm^{-1}Fe–O, 1158-894 cm^{-1} organic skeleton of chitosan and guar gum. Asymmetric stretching –CH,-CH_2 pyranose rings at 2924, 2864 cm^{-1}, 1658 cm^{-1}, Schiff's base, 3052 cm^{-1}, 3027 cm^{-1} (C–H, Ph); 1691 cm^{-1} C═N, 1600, 1575,1493 and 1454 cm^{-1}C═C Ph; 757, 692 cm^{-1} (benzyl group), 1250 cm^{-1} (epoxide), 1000 cm^{-1} C–H Stretching C═O in MePy overlapped with amide of CT at 1657 cm^{-1}, 2207, 2162, 1641 cm^{-1} nitrile [31].

Fig. 5 (a-e): SEM micrographs of showed chitosan (a) easily formulated with good compatibilit of chitosan with the main coating constituents (b: MePyr, c: silica, d:PhPyr and e: guar gum.

CT is chemically grafted at primary –OH and NH_2. All additives were dispersed in CT@GG binder [32]. Chitosan microstructure changed from rigid polymers chains into different morphology surface according to the nature of the additive. After immersion 1.0 h in 1.0 M HCl, outstanding and durability of coated sample is confirmed relative to bare metal surface is confirmed from SEM micrographs, Fig. 6.

SEM micrographs of S_4 hybrid coating loaded by Phpyr confirmed good surface morphology due to synergetic inhibiting by phenyl

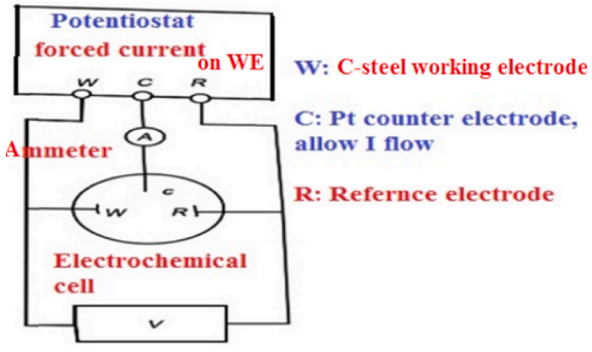

Fig. 3. Schematic representation for measuring corrosion rate.

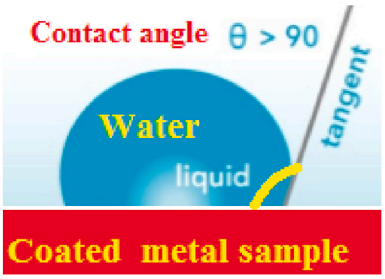

Fig. 4. Schematic representation of measuring contact angle.

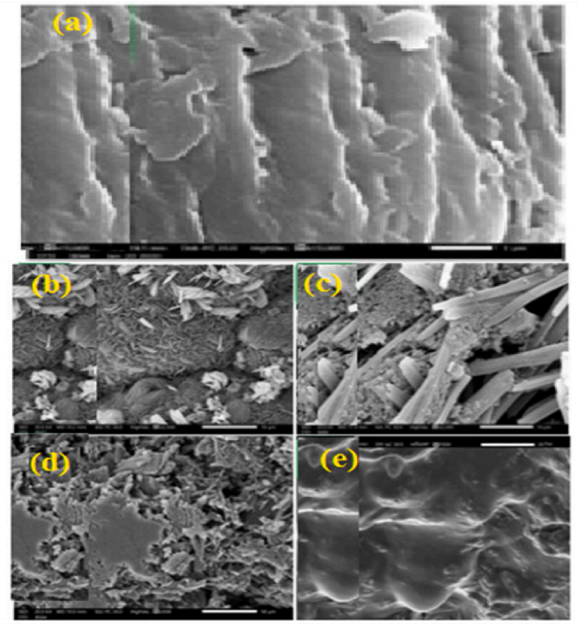

Fig. 5. Modification of chitosan morphology (a) on blending with: b) Me pyr, c) silica, d) Phpyr and e) guar gum.

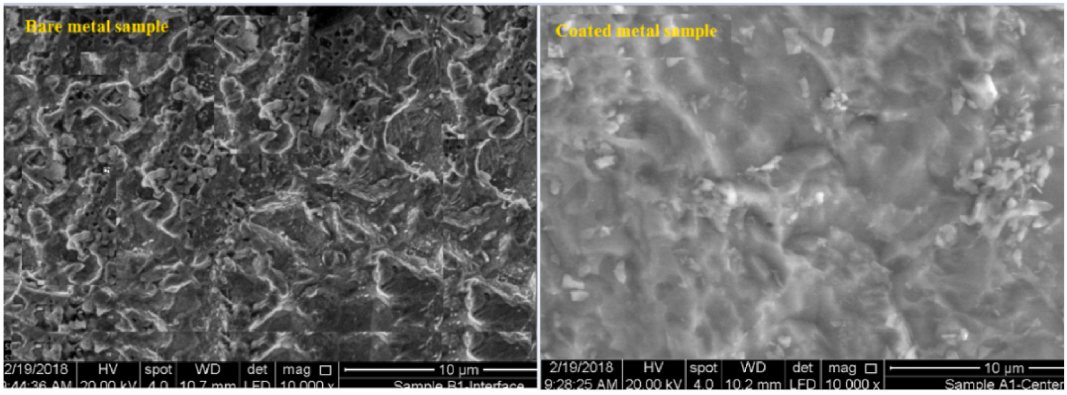

Fig. 6. Comparative surface morphology of bare and coated metal surface.

group of pyrimidine derivative. Silica filed pores and reinforced coating. Coating formulations contain multi-functional groups: NH_2, OH^- from CT and functional groups of pyrimidininon enabled formation of Schiff bases and polyesters [31].

Gloss of the coating sample 4 is due GG and coated silica in nanoscale size (1.5 mμ). The enhancing effect of silica on the gloss of the hybrid coating was confirmed by visual photographic images of coated metal surface by sample 4 in comparison to bare metal surface

and metal surface coated by chitosan film [32,33], Fig.SI2.

Synergism inhibition is achieved by adjusting nature, proportion, compatible constituents for homogeneous dispersion structure, functionality giving pure homogeneous, structurally tunable transparent insulating protective coating film. Soft posphorous atom of TPPC form with CT phosphouros = Nitrogen double bond giving anticorrosive primer coating resist wear. The delocalized electrons in conjugated hydrophobic phenyl groups improved protection. Citric acid cross linker contains planar carboxylic acid, $COOH^-$ and OH esterified alcoholic OH of CT@GG copolymer leaving NH_2 free to binding steel surface. Citric acid is more safer ecofriencly cross linker than benzoyl peroxide, radiation, silane improves chemical and thermal stability and resistance to shrinkage and stress cracking due to formed network. Silica regulated chains of chitosan@ GG binder *via* covalent bond formation with amino (NH_2) and (OH) groups of the binder. Hence silica increased stability to (thermal, mechanical stress), hardness, toughness and stiffness of resin coating by filling pores [28,34].

The biocidal activities of chitosan and pyrimidine derivatives were collected in Table 2.

The low MIC of CT and its composites for different tested bacteria and fungi species suggested applicability of these composites coating antimicrobial biocides for mitigating microbiologically induced corrosion (MIC) encountered in petroleum industries [23].

Pyrimines decreased MIC (more active than CT) [27].

Steady state equilibrium open circuit potential, E_{OCP} of C-steel attained after 20 min before impedance and polarization measurement, Fig. 7. All E_{OCP} are shifted to more noble compared to bare steel (520 mV versus SCE) [28].

Fig. 8 showed Nyquist impedance plots for coated C-steel sample in 1.0 M HCl have capacitive semicircles confirmed dielectric impermeable film coatings insulator and isolated metal surface. No diffusion tail observed at low frequency region indicating that corrosion is under charge transfer control. Bode impedance, Z at low frequency region plots confirmed coating performance, Fig. 9 [35].

Negative phase shift angle, θ (-80^o) for some representative coating samples [26]. Fig. 10 indicating alternating current I(ω) proceeds alternating voltage V(ω) and confirmed adherent coating film [35].

The phenyl group in Phpyr@CT-GG-silica increased protection efficiency of coating. The inset in Fig. 8 is equivalent circuit model simulated heterogeneous metal solution/interface used in nonlinear fitting of Nyquist plots with negligible error. Elements constant phase elements Q_{dl} and Q_f are capacitances of electrical double layer and coating film respectively. The parameter R_s resistance of solution between working electrode and reference electrode; R_f is the resistance of coating film; R_{ct} is the charge transfer resistance across metal surface [35]. All impedance parameters and heterogeniety constant of corrosion system,n are collected in Table 3.

Fig. 11 showed representative polarization curves for coated samples C-steel in 1.0 M HCl. Both the cathodic and anodic polarization curves were shifted to higher over-potentials with the larger shift in cathodic polarization curve, so the hybrid coating act as mixed-type inhibitors with predominant cathodic character [24]. Tafel behavior indicating that corrosion of steel in HCl is under activation control. Steel corrodes in HCl given soluble ferrous chloride, $FeC1_{2(aq.)}$ and hydrogen gas [28,35].

Coating inhibited rates of both anodic oxidation and cathodic reductions. Polarization parameters: Corrosion potential, $E_{corr.}$, corrosion current density, $i_{corr.}$, anodic-, and cathodic Tafel slops β_a, β_c respectively for coated C-steel samples are obtained using Tafel extrapolation method at ±50 mV around $E_{corr.}$, Table 4 [28].

%P from of coating samples from polarization and impedance are in good agreement above 99.9 %.

Ph pyr gave more dispersed coating film than MePyr due to more delocalized electrons on phenyl group. The optimum 3.0 % SG showed sufficient due to increased stiffness of coating film. Large 4 % SG declined polymer flexibility, decreased %P. Silica sealed pores in chitosan binder [12,30]. Functional N and O-groups of coating adsorbed on metal surface and protected it against corrosion. NH_2, OH^- donate free lone pairs of electrons to the vacant orbitals in steel surface form type coordinate. –Si–O, –C═C–, –COOH, $–NH_2$, –SH, –S–S–, –C═O. Examples are Schiff bases. NaOH cleaved hydrophobic ring of CT giving open structure C═N imine enhancing film formation [28]. TPPC provided P atom and hydrophobic phenyl groups and extensive electron density. Micelles of SDS solubilized coating constituents in water.

Fig. 13 showed representative adsorption-desorption isotherms of $N_{2\ (g)}$ on coated samples 6 and 7.

Low volume of adsorbed nitrogen confirmed that the coating functional groups C═O, C–O, –OH, NH_2, double bonds, etc. adsorbed on the metal surface [27]. Adsorption-desorption isotherms are type IV of little volume of adsorbed nitrogen confirmed negligible coating porosity. Linear BET plot ($\frac{P}{V\ (P^o-P)}$ versus $\frac{P}{V_a\ (P^o-P)}$ versus relative pressure $\left(\frac{P}{P^o}\right)$ (0.05–0.35) enabled calculation of monolayer volume (V_m) and adsorption constant from the slope and the intercept. T otal pore volume, pores area $\left(a_{S,BET}\right.$ calaculated using equation 2$\left.\right)$ and mean pore diameter of coatings decreased on loading SG on CT, as coated silica

Table 2
Minimum inhibitory concentrations (MIC) of tested samples as biocides.

Microorganism	Sample, MIC, ug/mL		
	Chitosan	Methyl pyr@chitosan	Phenylpyr@chitosan
B. Subtilis (ATCC 6633)	4.2	1.99	1.0
S.aureus (ATCC 6538)	8.3	8.1	4.2
E.coli (ATCC 8739)	31.9	15.9	8.2
P.aeruginosa (ATCC 90274)	16.2	8.2	4.2
C.albicans (ATCC 10221)	4.2	2.1	1.1

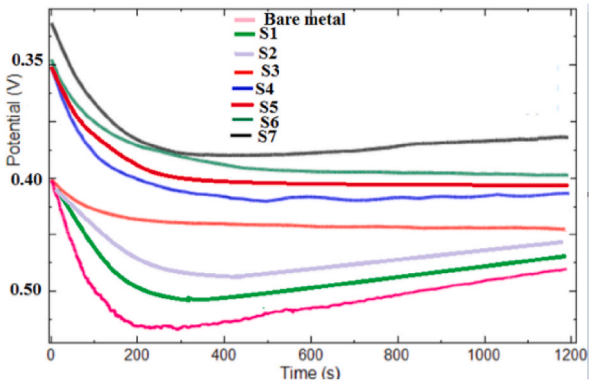

Fig. 7. Potential-time curves for coated sample C-steel in 1.0MHCl

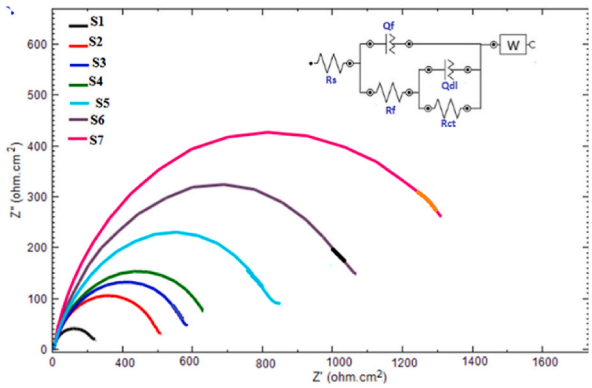

Fig. 8. Nyquist plots for coated C-steel in 1.0 M HCl.

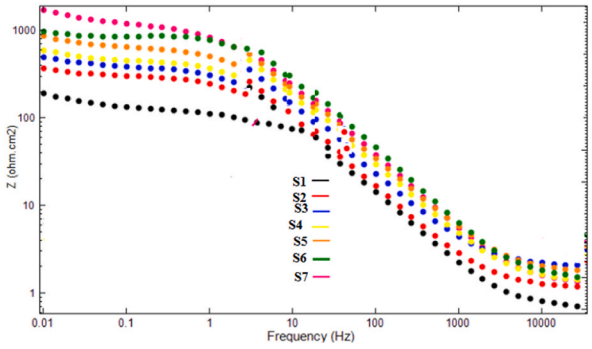

Fig. 9. Bode impedance plots for coated C-steel samples in 1.0MHCl

filled pores in CT@GG binder grafted by methyl or phenyl pyrimidinon [15] give micro pores [30].

$$\text{Specific surface area } \left(a_{S,BET}\right) = \frac{V_m\, \alpha N_A}{mass_{adsorbent}\, V_o} = \frac{V_m \times 16.6 * 6.023 * 10^{23}}{mass\, V_o} \tag{3}$$

Where α molecular and V_o are the surface area of the molar volume 22.414 L mol.$^{-1}$ of nitrogen respectively [27].

Both coating samples S6 and S7 showed slight porosity, Table 5.

Loading efficiency of silica on binder matrix was confirmed from comparison of particle size distribution of coating samples of S_4 and S_5 emulsion [36], Fig. 14.

Thermal stability of coatings of S4 and S5 was ascertained from the comparative thermal gravimetric analysis TGA (recording weight loss as a function of heating temperature, Fig. 15 (a, b).

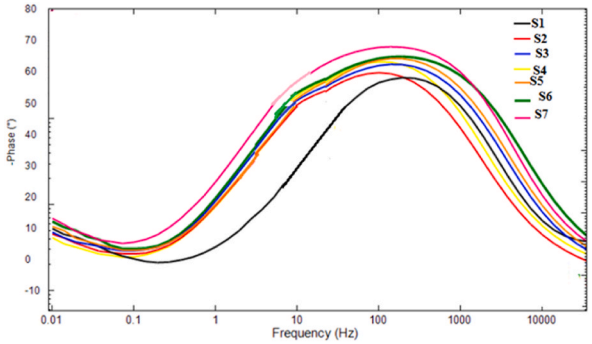

Fig. 10. Phase shift plots of some coated samples: a) S_4, b) S_6 and c) S_7.

Table 3
Impedance paramters for coated samples in 1.0 M HCl.

Sample	R_{ct} Ohm.cm^2	R_s Ohm.cm^2	n	Q_{dl} μF. cm^{-2}	R_f Ohm.cm^2	n_f	C_f μF. cm^{-2}	%P
Blank	1.30	0.91	0.91	5189	–	–	–	–
CT@GG	360	0.97	0.91	127	17.94	0.72	100	99.6
1%silica	510	0.96	0.85	137	6.471	0.84	44	99.7
2%silica	609	0.89	0.84	121	8.541	0.88	38	99.8
3%silica	690	0.82	0.90	100	8.881	0.88	13	99.8
4%silica	880	0.99	0.87	68	7.841	0.94	27	99.9
4%silica + MePyr	1101	1. 1	0.95	60	9.191	0.89	9	99.9
4%silica + PhPyr	1486	1.2	0.92	58	19.80	0.90	7	99.9

The parameter (n) ranged from 0.9 to 1 confirmed heterogeneity of corrosion system [25]. The decrease in Q_{dl} approved adsorption of active ingredients of coating on metal surface.

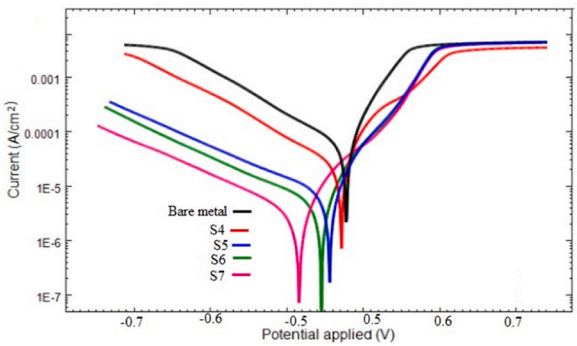

Fig. 11. Polarization curves for bare and coated C-steel samples in 1.0 M HCl.

At the same chemical constituents of coating, increasing %wt. of coated silica from 3 % to 4 % increased thermal stability in terms of residual weight loss (residual wt.%) 3.817 % and 21.72 % for 3 % and 4 % coated silica respectively. The alkali media was necessary for CT to form insulating surface film. NaOH opened CT hydrophobic ring giving imine C═NH bond intercalation by pyrimidinons [37]. Grafted CT is thermally stable.

DSC thermal transition of coating (4%silica + PhPyr@CT-GG), Fig. 16.

Coating is thermally stable showed all higher temperature of phase transition (T glassy (only increase heat capacity), $T_{crystallization}$ (incresaes kinetic energy of ordered crystals and Tmelting (causes solid-liquid equilibrium [37].

All coated samples water contact angles (WCA) above 150°, Fig. 17 indicating hydrophobicity and no water spreading on coating surface.

Coating silica particles caused surface roughness improved hydrophobic characteristics of coating surface [29]. Rough hierarchical structure creates repellence with water due to entrapped air pockets formed between surface grooves and water.

Protection mechanism could be explored as coating adhesion prevents penetration of localized corrosive electrolyte pockets under coat. Metal/polymeric coating interface involve physical and chemical adsorption of molecules of polymers and corrosion inhibitor; chemical reaction between both chitosan@GG and Pyrimindones with metal surface; mechanical interlocking polymer molecules into

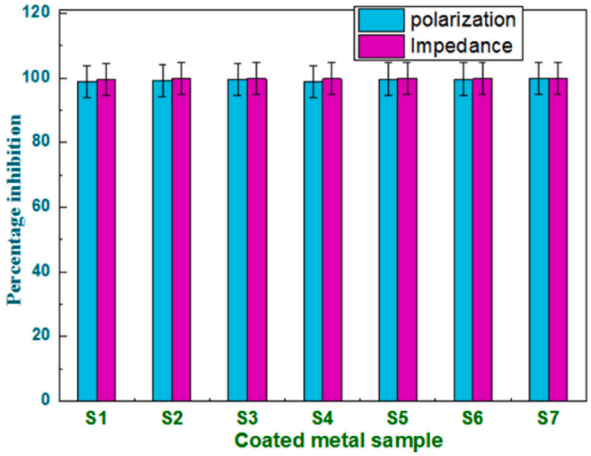

Fig. 12. Comparative %P of the coated steel samples.

Table 4
Polarization parameters of C-steel samples in 1.0 M HCl.

Sample	β_a	$-\beta_c$	$i_{corr.}$ (mA.cm^{-2})	$E_{corr.}$(mV)	%P
	(mV.decade^{-1})				
Bare	90	88	6.70	501	–
CT@GG	42	205	0. 07	422	99.0
1%silica	43	211	0.05	412	99.3
2%silica	46	212	0.03	392	99.6
3%silica	48	211	0.03	395	99.7
4%silica	50	207	0.02	391	99.7
4%silica + MePyr	51	215	0.02	392	99.9
4%silica + PhPyr	53	230	0.01	385	99.9

Coating shifted $E_{corr.}$ of steel to more noble potential relative to bare steel in 1.0 M HCl. Fig. 12 showed comparative % P of coating sample calculated from impedance and polarization measurements [28].

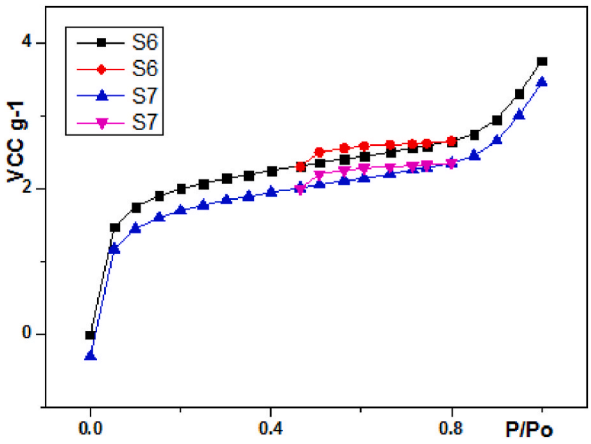

Fig. 13. Adsorption-desorption isotherms of $N_{2\ (g)}$ on steel surface coated by samples S_6, S7.

pores on metal surface; electrostatic interaction of functional groups C═O, C–O, –OH, NH_2, COOH and oppositely charged metal surface. Each mechanism operates under certain conditions. Adsorption predominates where polymer adheres to metal surface or metal oxide surface film *via* Lewis acid base interaction. Free NH_2, OH chelates metal surface. P from TPPB and H_3PO_3 form double bond with N atoms of CT. SG reinforcing agent binding CT chains *via* oxygen atom. Low electron negative Si increased delocalized electron density. SG regulate CT chains [28,35].

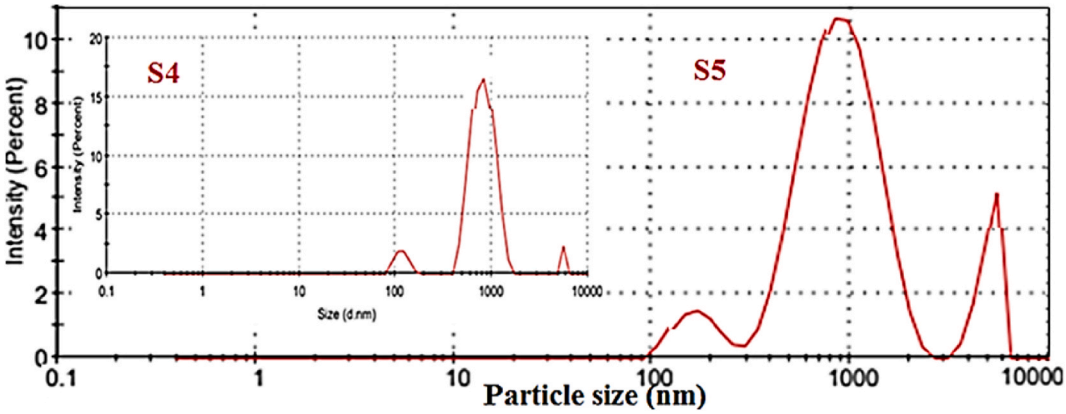

Fig. 14. Particle size distribution of coating samples S4(inset) and S5.

Table 5
Pore parameters of some coated samples.

Sample	$a_{S,\ BET}$ (m^2g^{-1})	Pore diameter (nm)	Pore volume	V_m ($CC.g^{-1}$)	Adsorption constant (C)	Δ H_{ads} ($J.mol^{-1}$)	Δ H_1
S6	4.0	3.08	0.04	9.10	11.0	581.3	10878
S7	3.32	3.01	0.02	7.12	9.95	478.0	5988

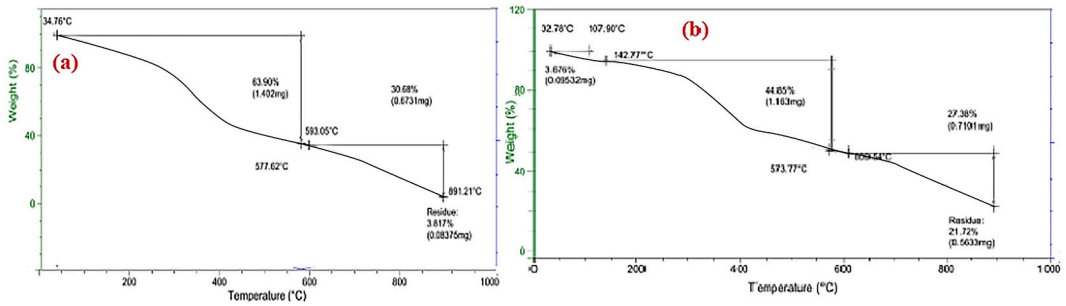

Fig. 15. Comparative thermograms for CT@additives:(a) 3 %, (b) 4 % coated silica respectively.

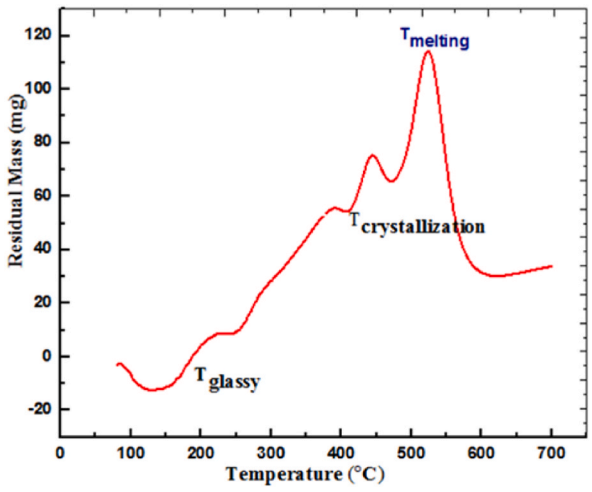

Fig. 16. Thermal response of coating sample: 4%silica + PhPyr@CT-GG

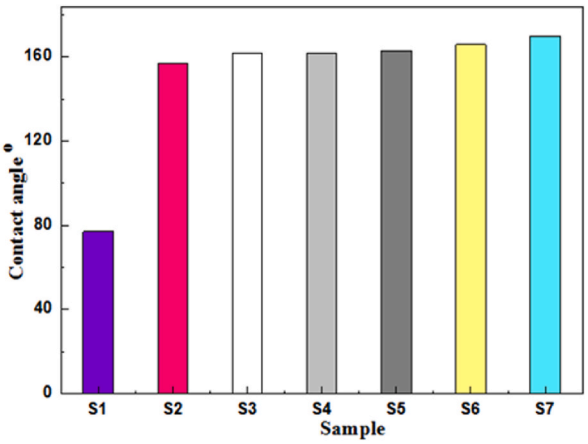

Fig. 17. Contact angle of coating samples.

4. Conclusion

This study provided new protective (for C-steel during acid pickling) hydrophobic coating of chitosan@ guar gum binder reinforced by coated silica and coating aids. Synergism inhibition was achieved by rendering CT as resin binder using low coat available modifiers. The hot melt coated was easily formulated, applied and cured through simple chemical reactions involving functional groups of all coating constiuents. The coated silica decreased water spreading on coated sample and enhancing thermal stability and mechanical strength due to filling pores in binder. Silica modified particle size distribution and decreased pore size and reduce the coating permeability.

Ethics approval and consent participation@ publication

No Ethical issue. Authors approved consent on participation and publication

Data availability statement

"All data generated or analysed during this study are included in this published article".

CRediT authorship contribution statement

Salam N.Hattawi: Writing – review & editing, Visualization, Funding acquisition. **Ahmed G. Ahmed:** Writing – original draft, Validation, Funding acquisition. **Firas M. Fadhil:** Writing – original draft, Investigation, Funding acquisition. **Stephen R. Kuot:** Methodology, Investigation, Formal analysis, Data curation. **Mai S Alsubaie:** Writing – original draft, Resources, Investigation. **Mohammed L.Alazmi:** Resources, Investigation, Funding acquisition. **H.A. Fetouh:** Writing – review & editing, Writing – original draft, Visualization, Validation, Supervision, Software, Investigation, Formal analysis, Data curation, Conceptualization.

Declaration of competing interest

The authors declare the following financial interests/personal relationships which may be considered as potential competing interests:Authors declared no conflict of interest have influenced the submitted work If there are other authors, they declare that they have no known competing financial interests or personal relationships that could have appeared to influence the work reported in this paper.

Appendix A. Supplementary data

Supplementary data to this article can be found online at https://doi.org/10.1016/j.heliyon.2024.e33743.

References

[1] H.M.H. Farh, M.E.A.B. Seghier, T. Zayed, A comprehensive review of corrosion protection and control techniques for metallic pipelines, Eng. Fail. Anal. 143 (2023) 106885.

[2] K. Thakur, S. Gharde, S. Jamdade, B. Kandasubramanian, Hydrophobic and super-hydrophobic polymer coatings, in: Smart Polymers, CRC Press, 2022, pp. 225–244.
[3] A. Kumar, J. Jaiswal, K. Tsuchiya, R.S. Mulik, Modern coating processes and technologies, in: Coating Materials: Computational Aspects, Applications and Challenges, Springer Nature Singapore, Singapore, 2023, pp. 33–80.
[4] M.M.H. Tusher, A. Imam, M.S.I. Shuvo, Future and challenges of coating materials, in: Coating Materials: Computational Aspects, Applications and Challenges, Springer Nature Singapore, Singapore, 2023, pp. 229–251.
[5] W. Li, Y. Zhan, S. Yu, Applications of superhydrophobic coatings in anti-icing: theory, mechanisms, impact factors, challenges and perspectives, Prog. Org. Coating 152 (2021) 106117.
[6] M.H. Nazari, Y. Zhang, A. Mahmoodi, G. Xu, J. Yu, J. Wu, X. Shi, Nanocomposite organic coatings for corrosion protection of metals: a review of recent advances, Prog. Org. Coating 162 (2022) 106573.
[7] G. Cui, Z. Bi, S. Wang, J. Liu, X. Xing, Z. Li, B. Wang, A comprehensive review on smart anti-corrosive coatings, Progress in organic coatings 148 (2020) 105821.
[8] S. Zehra, M. Mobin, J. Aslam, An overview of the corrosion chemistry. Environmentally Sustainable Corrosion Inhibitors, 2022, pp. 3–23.
[9] M. Montazerian, F. Hosseinzadeh, C. Migneco, M.V. Fook, F. Baino, Bioceramic coatings on metallic implants: an overview, Ceram. Int. 48 (7) (2022) 8987–9005.
[10] K.Y. Guo, Q. Wu, M. Mao, H. Chen, G.D. Zhang, L. Zhao, J.F. Gao, P. Song, L.C. Tang, Water-based hybrid coatings toward mechanically flexible, super-hydrophobic and flame-retardant polyurethane foam nanocomposites with high-efficiency and reliable fire alarm response, Compos. B Eng. 193 (2020) 108017.
[11] M. Torabi-Kaveh, M. Moshrefyfar, S. Shirzaei, S.M.A. Moosavizadeh, B. Ménendez, S. Maleki, Application of resin-TiO2 nanoparticle hybrid coatings on travertine stones to investigate their durability under artificial aging tests, Construct. Build. Mater. 322 (2022) 126511.
[12] B.O. Alan, M. Barisik, H.G. Ozcelik, Roughness effects on the surface charge properties of silica nanoparticles, J. Phys. Chem. C 124 (13) (2020) 7274–7286.
[13] X. Li, Y. Peng, F. Zhang, Z. Yang, Z. Dong, Fast-response, no-pretreatment, and robustness air-water/oil amphibious superhydrophilic-superoleophobic surface for oil/water separation and oil-repellent fabrics, Chem. Eng. J. 427 (2022) 132043.
[14] E. Mięków, M. Cichomski, M. Zieliński, T. Klepka, D. Sroczyński, A. Fenyk, Tests of physicochemical and mechanical strength properties of polymer composites on an epoxy resin matrix, modified by a constant magnetic field, Materials 15 (19) (2022) 6730.
[15] B.K. Kandola, F. Magnoni, J.R. Ebdon, Flame retardants for epoxy resins: application-related challenges and solutions, J. Vinyl Addit. Technol. 28 (1) (2022) 17–49.
[16] R.P. Chaudhary, C. Parameswaran, M. Idrees, A.S. Rasaki, C. Liu, Z. Chen, P. Colombo, Additive manufacturing of polymer-derived ceramics: materials, technologies, properties and potential applications, Prog. Mater. Sci. 128 (2022) 100969.
[17] G. Martínez-Barrera, A. Martínez-López, E. Vigueras-Santiago, M. Martínez-López, Effects of gamma radiation on the physicochemical properties of polyester resin and its use in composite materials. Recycled Polyester: Manufacturing, Properties, Test Methods, and Identification, 2020, pp. 15–28.
[18] Y. Zheng, Y. Gao, H. Li, M. Yan, J. Zhao, Z. Liu, Chitosan-acrylic acid-polysuccinimide terpolymer as environmentally friendly scale and corrosion inhibitor in artificial seawater, Desalination 520 (2021) 115367.
[19] H.A. Elbadawy, A. El-Dissouky, S.M. Hussein, S.R. El-Kewaey, S.A. Elfeky, G. El-Ghannam, A novel terpolymer nanocomposite (carboxymethyl β-cyclodextrin–nano chitosan–glutaraldehyde) for the potential removal of a textile dye acid red 37 from water, Front. Chem. 11 (2023) 1115377.
[20] L.M. Anaya-Esparza, J.M. Ruvalcaba-Gómez, C.I. Maytorena-Verdugo, N. González-Silva, R. Romero-Toledo, S. Aguilera-Aguirre, A. Pérez-Larios, E. Montalvo-González, Chitosan-TiO2: a versatile hybrid composite, Materials 13 (4) (2020) 811.
[21] M.H. Lin, Y.H. Wang, C.H. Kuo, S.F. Ou, P.Z. Huang, T.Y. Song, Y.C. Chen, S.T. Chen, C.H. Wu, Y.H. Hsueh, F.Y. Fan, Hybrid ZnO/chitosan antimicrobial coatings with enhanced mechanical and bioactive properties for titanium implants, Carbohydr. Polym. 257 (2021) 117639.
[22] G. Cavallaro, S. Micciulla, L. Chiappisi, G. Lazzara, Chitosan-based smart hybrid materials: a physico-chemical perspective, J. Mater. Chem. B 9 (3) (2021) 594–611.
[23] X. He, S. Li, R. Shen, Y. Ma, L. Zhang, X. Sheng, Y. Chen, D. Xie, J. Huang, A high-performance waterborne polymeric composite coating with long-term anti-corrosive property based on phosphorylation of chitosan-functionalized Ti 3 C 2 T x MXene, Adv. Compos. Hybrid Mater. (2022) 1–13.
[24] H.S. Bahari, F. Ye, E.A.T. Carrillo, C. Leliopoulos, H. Savaloni, J. Dutta, Chitosan nanocomposite coatings with enhanced corrosion inhibition effects for copper, Int. J. Biol. Macromol. 162 (2020) 1566–1577.
[25] Z. Yu, J. Hu, H. Meng, A review of recent developments in coating systems for hot-dip galvanized steel, Frontiers in Materials 7 (2020) 74.
[26] H.A. Fetouh, H.M. Abd-Elnaby, M.S. Alsubaie, E.R. Sallam, New experimental low-cost nanoscience technology for formulation of silver nanoparticles-activated carbon composite as a promising antiviral, biocide, and efficient catalyst, J. Exp. Nanosci. 17 (1) (2022) 297–314.
[27] E.R. Sallam, S.F. Aboulnaga, A.M. Samy, D.M. Beltagy, J.M. El Desouky, H. Abdel-Hamid, H.A. Fetouh, Synthesis, characterization of new heterocyclic compound: pyrazolyl hydrazino quinoxaline derivative: 3-[5-(hydroxy1methyl)-1-phenylpyrazol-3-yl]-2-[2, 4, 5-trimethoxybenzylidine] hydrazonyl-quinoxaline of potent antimicrobial, antioxidant, antiviral, and antitumor activity, J. Mol. Struct. 1271 (2023) 133983.
[28] M. Elbatouti, H.A. Fetouh, Extraction of eco-friendly and biodegradable surfactant for inhibition of copper corrosion during acid pickling, Adsorpt. Sci. Technol. 37 (7–8) (2019) 649–663.
[29] R.S. Almufarij, H.A. Fetouh El Sayed, M.E. Mohamed, Eco-friendly approach for the construction of superhydrophobic coating on stainless steel metal based on biological metal–organic framework and its corrosion resistance performance, Materials 16 (13) (2023) 4728.
[30] V.G. Baldovino-Medrano, V. Niño-Celis, R. Isaacs Giraldo, Systematic analysis of the nitrogen adsorption–desorption isotherms recorded for a series of materials based on microporous–mesoporous amorphous aluminosilicates using classical methods, J. Chem. Eng. Data 68 (9) (2023) 2512–2528.
[31] A.A. Assiry, M.I. Karobari, G.S.S. Lin, R. Batul, N.T. Snigdha, A.M. Luke, K.P. Shetty, G.A. Scardina, T.Y. Noorani, Microstructural and elemental characterization of root canal sealers using FTIR, SEM, and EDS analysis, Appl. Sci. 13 (7) (2023) 4517.
[32] N. Li, Y. Zhang, P. Li, B. Zhu, W. Wang, Z. Xu, Enhanced permeability and biofouling mitigation of forward osmosis membranes via grafting graphene quantum dots, Front. Chem. Sci. Eng. 17 (10) (2023) 1470–1483.
[33] J.M. James, I.W. Taifa, Quality improvement of long oil alkyd (LOA) resin requirements in the formulation of Hi-gloss paints, Int. J. Qual. Reliab. Manag. 40 (7) (2023) 1753–1776.
[34] A.S. Gnedenkov, S.L. Sinebryukhov, V.S. Filonina, A.Y. Ustinov, S.V. Gnedenkov, Hybrid coatings for active protection against corrosion of Mg and its alloys, Polymers 15 (14) (2023) 3035.
[35] R.M. Keshk, G.E.A. Elgawad, E.R. Sallam, M.S. Alsubaie, H.A. Fetouh, Synthesis and characterization of nicotinonitrile derivatives as efficient corrosion inhibitors for acid pickling of brass alloy in nitric acid, ChemistrySelect 7 (33) (2022) e202202678.
[36] R.S. Riseh, M. Vatankhah, M. Hassanisaadi, J.F. Kennedy, Chitosan/silica: a hybrid formulation to mitigate phytopathogens, Int. J. Biol. Macromol. (2023) 124192.
[37] I. Khan, I. Khan, K. Saeed, N. Ali, N. Zada, A. Khan, F. Ali, M. Bilal, M.S. Akhter, Polymer nanocomposites: an overview, Smart Polymer Nanocomposites (2023) 167–184.